Metal–organic frameworks with wine-rack motif: What determines their flexibility and elastic properties?

Aurélie U. Ortiz,[1] A. Boutin,[2] Alain H. Fuchs,[1] and François-Xavier Coudert[1,a)]
[1]*CNRS and Chimie ParisTech, 11 rue Pierre et Marie Curie, 75005 Paris, France*
[2]*CNRS-ENS-UPMC, Département de Chimie, École Normale Supérieure, 24 rue Lhomond, 75005 Paris, France*

(Received 18 February 2013; accepted 9 April 2013; published online 1 May 2013)

We present here a framework for the analysis of the full tensors of second-order elastic constants of metal–organic frameworks, which can be obtained by *ab initio* calculations. We describe the various mechanical properties one can derive from such tensors: directional Young's modulus, shear modulus, Poisson ratio, and linear compressibility. We then apply this methodology to four different metal–organic frameworks displaying a wine-rack structure: MIL-53(Al), MIL-47, MIL-122(In), and MIL-140A. From these results, we shed some light into the link between mechanical properties, geometric shape, and compliance of the framework of these porous solids. We conclude by proposing a simple criterion to assess the framework compliance, based on the lowest eigenvalue of its second-order elastic tensor. © *2013 AIP Publishing LLC*. [http://dx.doi.org/10.1063/1.4802770]

I. INTRODUCTION

Metal–organic frameworks (or MOFs) are crystalline microporous materials whose three-dimensional framework is constructed from metal centers linked together by organic ligands. They display a large structural diversity and chemical versatility, enabling the design of new materials with tunable host–guest properties. For this reason, they have vast potential for use in industrial processes for gas separation and storage, sensing, and catalysis. One fascinating subclass of MOFs are the flexible MOFs, also called Soft Porous Crystals (SPCs),[1] which behave in a remarkable stimuli-responsive fashion.[2] SPCs feature dynamic crystalline frameworks displaying reversible single-crystal-to-single-crystal structural transformations of large amplitude under a number of external physical constraints such as guest adsorption, temperature, or mechanical pressure. The number of such materials reported in the literature is rapidly growing, as is the number of both experimental and theoretical studies of their physicochemical properties. Many facets of the structural transitions of SPCs have been the subject of a large research effort, including structural determination of the material's phases (both experimentally[3] and by first principles calculations[4]), the energetics[5,6] of adsorption-induced transitions and their thermodynamics.[7,8]

While the elastic properties of some "rigid" MOFs have been well characterized (either by quantum chemistry calculations[9] or force field-based molecular dynamics[10]), it is only recently that the mechanical behavior of soft porous crystals has been addressed. In 2010, Neimark *et al.*[11] proposed that mechanical stress exerted onto the MOF framework upon adsorption be considered the key quantity in determining the occurrence of adsorption-induced structural transitions. In that view, the phase transitions of the host material would take place when stress reached a certain "stress threshold" that a given structure cannot withstand. Later in 2010, Beurroies *et al.*[12] published the first experimental demonstration that the structural transitions between two phases of a SPC (in this case, material MIL-53(Cr)) could be induced by uniform mechanical compression of the sample by a nonpenetrating fluid, using the process known as mercury porosimetry. This was shown to be in good agreement with the "stress threshold" hypothesis, and allowed the estimation of bulk modulus constants for both phases of the MIL-53(Cr) material,[13] the first time for a flexible MOF to our knowledge. Molecular simulation was very recently used to confirm this estimate,[14] and a different compression technique (powder X-ray diffraction upon compression) was used to measure the bulk modulus of related material NH_2-MIL-53(In).[15] Nevertheless, these measurements of the scalar bulk modulus fail to account for the tensorial nature of the generalized Hooke's law that governs elastic deformations of the solid. In order to bring further insight into the elastic behavior of SPCs, we recently showcased how the calculation of the full tensor of elastic constants of the MIL-53 and DMOF-1 materials can be used to characterize their flexibility (the so-called "breathing" phenomenon).[16] We further showed that flexible MOFs with lozenge-shaped one-dimensional channels exhibited highly anisotropic Young's and shear modulus, as well as spectacular negative linear compressibility. At the same time, Ogborn *et al.* hypothesized that frameworks of the MIL-53 type would exhibit very strong anisotropic positive/negative linear compressibility.[17]

In this paper, we use first principles calculations of the elastic constants of a series of metal–organic frameworks displaying the same wine-rack (or trellis fencing) motif, which has been widely studied in dense inorganic materials for being the source of unusual elastic properties including negative linear compressibility (NLC). NLC is a relatively rare phenomenon in inorganic crystals and is often associated with a

a)Electronci mail: fx.coudert@chimie-paristech.fr

limited number of basic structural motifs,[18] among which the wine-rack topology is chief.[19,20] For this reason, we investigate here the existence of anomalous mechanical properties of MOFs based on the wine-rack connectivity. From the full tensorial analysis of the elastic constants, we calculate physical properties of interest: directional Young's modulus, shear modulus, Poisson's ratio, and linear compressibility. We show that, while anisotropy of these elastic properties is inherent to the wine-rack motif of these metal–organic frameworks, the existence of soft deformation modes can be linked to the existence of possible structural transitions in the material in presence of an external stimulus.

II. METHODS

We performed density functional theory calculations of the tensor of elastic constants of two new MOF structures: MIL-122(In) and MIL-140A. The structures of these frameworks, as well as those of MIL-53(Al) and MIL-47 with which we compare them, are presented in Fig. 1, and their unit cell parameters are summarized in Table I. In Secs. II A–II C, we explain the details of our calculations.

A. First principles calculations

The structures of all MOF materials considered were fully relaxed by optimizing both atomic positions and unit cell parameters, starting from the experimental crystallographic structure. We performed first principles calculations in the density functional theory approach with periodic unit cell, full use of the crystals' symmetry elements and localized basis sets as implemented in the CRYSTAL09 code.[21] We used the B3LYP hybrid exchange-correlation functional,[22] with empirical correction for the dispersive interactions following the "D2" scheme of Grimme.[23] All electron basis sets were used for H, C, O, Al, V, and Zr, while a Durand and Barthelat pseudopotential was used for In. The accuracy of this methodology is now well established for the calculation of MOF structures,[24] energies,[6] and elastic constants.[25,26]

TABLE I. Space group (S.G.), unit cell parameters (a, b, c, and β) and volume (V) of the energy-minimized structures of the MOFs studied in this work.

Structure	S.G.	a (Å)	b (Å)	c (Å)	β (°)	V (β^3)
MIL-53(Al)-lp	*Imma*	16.48	6.68	13.24	90	1458.0
MIL-47	*Pnma*	6.79	16.05	13.98	90	1524.1
MIL-122(In)	$P2_1/c$	9.93	9.89	7.13	93.01	698.9
MIL-140A	$C2/c$	24.98	11.24	7.69	104.95	2086.9

B. Calculation of elastic constants

The tensorial Hooke's law establishes a general relationship between the strain ε and the stress σ in a solid in the linear elastic regime, through the fourth-order tensor $\mathbf{C}$ of second-order elastic constants[27]

$$\sigma_{ij} = \sum_{kl} \mathbf{C}_{ijkl}\varepsilon_{kl}, \tag{1}$$

where indices i, j, k, l run between 1 and 3. Taking advantage of the symmetries of stress and strain matrices and using the Voigt notation, the elasticity tensor (or stiffness tensor) $\mathbf{C}_{ijkl}$ can be expressed as a 6×6 symmetric matrix of 21 elastic constants C_{ij}, where i and j now run between 1 and 6 (in Voigt's notation, pair of indices are grouped as follows: 11→1, 22→2, 33→3, 23→4, 13→5, 12→6; this yields a one-index notation for σ and ε, and a two-indices notation

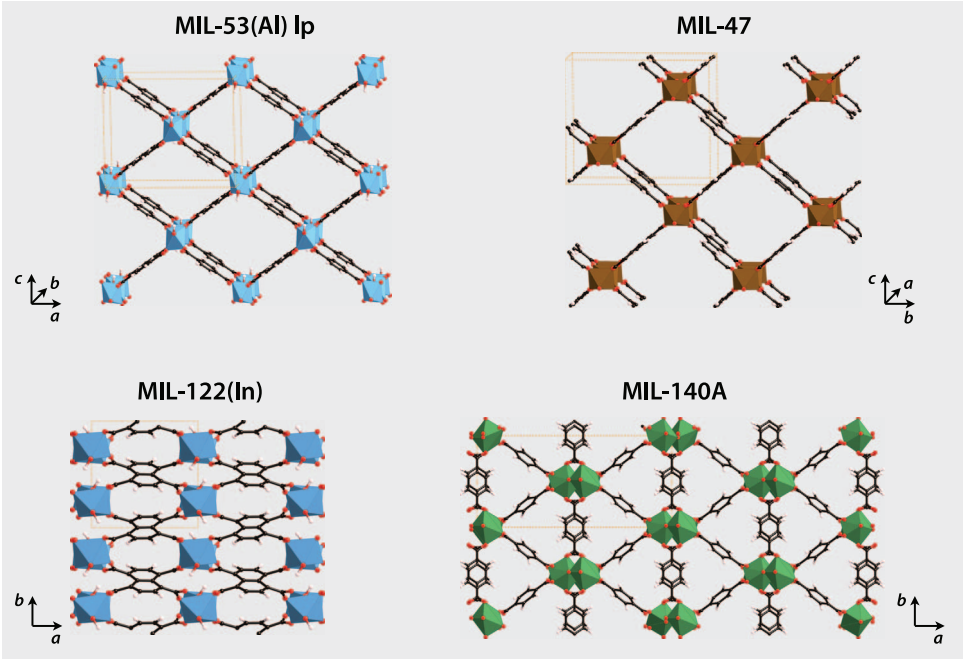

FIG. 1. Structures of MIL-53(Al)-lp, MIL-47, MIL-122(In), and MIL-140A. Metallic centers are represented as tetrahedra. Color code: C – black, O – red, H – white, Al – cyan, V – brown, In – blue, Zr – green.

for C). The crystal system of the material considered yields additional symmetry constraints, further reducing the number of independent elastic constants. The stiffness tensor of a monoclinic crystal involves 13 elastic constants

$$C_{\text{monoclinic}} = \begin{pmatrix} C_{11} & C_{12} & C_{13} & & C_{15} & \\ \cdot & C_{22} & C_{23} & & C_{25} & \\ \cdot & \cdot & C_{33} & & C_{35} & \\ & & & C_{44} & & C_{46} \\ \cdot & \cdot & \cdot & & C_{55} & \\ & & & \cdot & & C_{66} \end{pmatrix}, \quad (2)$$

while that of an material with orthorhombic lattice requires 9 elastic constants

$$C_{\text{ortho}} = \begin{pmatrix} C_{11} & C_{12} & C_{13} & & & \\ \cdot & C_{22} & C_{23} & & & \\ \cdot & \cdot & C_{33} & & & \\ & & & C_{44} & & \\ & & & & C_{55} & \\ & & & & & C_{66} \end{pmatrix} \quad (3)$$

(in this notation, dots are used to indicate nonzero elements constrained by the symmetric nature of the tensor).

The calculation of second-order elastic constants of the materials studied were performed with the use of the CRYSTAL09 code,[21] whose implementation was detailed in Ref. 25. Starting from the optimized geometry of the relaxed crystal, each deformation mode $\{\varepsilon_i, i = 1 \ldots 6\}$ is considered in turn.[28] For each deformation mode i, $2n$ strained structures are constructed with small deformations equal to $\varepsilon_k = k\delta\varepsilon_i$, with $-n \leq k \leq n$. δ, the increment of strain used, and n are parameters of this procedure. Each of the strained structures is geometry-optimized at fixed unit cell, and the converged crystal is used for an analytical calculation of the energy derivative with respect to unit cell parameters: $\frac{\partial E}{\partial \varepsilon_j}|_{\varepsilon_k}\ \forall j$. This series of derivatives along a single mode of deformation is then fitted as a function of k, which amounts to a finite difference calculation of the second derivatives $\frac{\partial^2 E}{\partial \varepsilon_i \partial \varepsilon_j}$. From these, the second-order elastic constants can be calculated by

$$C_{ij} = \frac{1}{V}\left(\frac{\partial^2 E}{\partial \varepsilon_i \partial \varepsilon_j}\right). \quad (4)$$

In this scheme using a mix of analytical derivatives and finite differences, each deformation mode ε_i allows the calculation of one row of the elastic constant matrix C.

The size of deformations used (δ) and total number of points sampled for each deformation mode (n) were varied to check the robustness of the method, as well as the fact that the strains imposed were within the limits of the elastic region. The elastic constants reported in this paper were typically obtained with $n = 5$ points and $\delta = 0.005$. In addition, we also checked the impact of using Grimme's D2 corrections for dispersive interactions on the values of the elastic constants calculated, because Grimme's empirical method is known to overestimate van der Waals interactions. We found that the elastic constants display a very small sensitivity to the use of the dispersion correction, with variations less than 3%. We concluded that while Grimme's dispersion corrections play a crucial role in comparing structures of different density (or unit cell volume), as shown, e.g., in Ref. 6, they have a smaller impact on local properties, including elastic moduli.

C. Tensorial analysis of the elastic constants

From the second-order elastic constants of each material, calculated as per Sec. II B, a full tensorial analysis was performed[29] and key quantities were derived that characterize the mechanical behavior of the structure in the elastic regime. In this section, we describe this analysis; the source code we used is available as a *Mathematica*[30] notebook as part of the supplementary material.[31]

The first analysis is to check that the Born elastic stability criterion holds true. This requires that the elastic constant tensor C be positive definite, i.e., that its eigenvalues all be strictly positive.[27,32] This is the generalization of the well-known stability criteria for cubic crystals

$$C_{44} > 0\ ;\ C_{11} - C_{12} > 0\ ;\ C_{11} + 2C_{12} > 0 \quad (5)$$

to other crystal systems.

We then calculate the compliance matrix S (and the related fourth-order tensor S) as the inverse of C (respectively, C). From this, we can calculate the directional Young's modulus for the crystal. Young's modulus $E(\mathbf{u})$, also known as the tensile modulus, is defined as the ratio of the uniaxial stress over the uniaxial strain along unit vector $\mathbf{u}$ (schematized in Fig. 2). In other words, it quantifies the deformation of the material in a direction, when it is compressed in that same direction. Young's modulus along the Cartesian x axis can be expressed in terms of the compliance matrix as $E_x = 1/\mathsf{S}_{1111}$. By applying the tensor rotation formula,[29] we can express from this the Young modulus in any direction $\mathbf{u}$ as

$$E(\mathbf{u}) = \frac{1}{u_i u_j u_k u_l \mathsf{S}_{ijkl}}, \quad (6)$$

where Einstein's notation of summation over repeated indices is adopted. The linear compressibility $\beta(\mathbf{u})$ can be expressed in a similar manner

$$\beta(\mathbf{u}) = u_i u_j \mathsf{S}_{ijkk}. \quad (7)$$

It characterizes the compression along axis $\mathbf{u}$ when the crystal undergoes an isotropic compression. Because both $E(\mathbf{u})$ and $\beta(\mathbf{u})$ are functions of a single unit vector $\mathbf{u}$, which can be parametrized by two angles θ and ϕ in spherical coordinates, they can be plotted in 3D as a "spherical plot," i.e., a parametric surface with radius $E(\theta, \phi)$, $0 \leq \theta \leq \pi$, $0 \leq \phi < 2\pi$.

Some other elastic properties are more complex, and depend on a second unit vector $\mathbf{v}$, perpendicular to $\mathbf{u}$. That is the

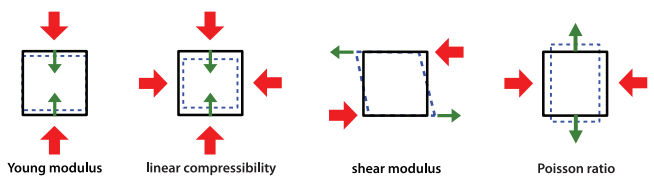

FIG. 2. Scheme of the directional elastic properties calculated in this work. For each, large red arrows represent the direction of applied stress and smaller green arrows the direction along which the resulting strain is calculated.

TABLE II. Minimal and maximal values as well as anisotropy of Young's modulus, shear modulus, linear compressibility, and Poisson's ratio for the MOFs studied, obtained by quantum chemistry calculations. Anisotropy of X is denoted by $A_X = X_{\max}/X_{\min}$.

Material	$E_{\min}$ (GPa)	$E_{\max}$ (GPa)	A_E	$G_{\min}$ (GPa)	$G_{\max}$ (GPa)	A_G	β_x (TPa^{-1})	β_y (TPa^{-1})	β_z (TPa^{-1})	$\nu_{\min}$	$\nu_{\max}$
MIL-53(Al)-lp	0.9	94.7	105	0.35	39.5	112	− 257	11	445	− 2.4	1.9
MIL-47	0.9	96.6	108	0.29	50.8	175	22	− 201	283	− 1.5	2.2
MIL-122(In)	42.3	160.4	3.8	12.5	48.1	3.8	− 1.9	17.5	7.7	− 0.2	0.7
MIL-140A	2.5	80.1	31.8	0.65	23.4	36.2	11.1	6.4	13.4	− 0.7	1.6

case of the shear modulus (or modulus of rigidity) $G(\mathbf{u}, \mathbf{v})$, which quantifies the material's response to shearing strains along $\mathbf{u}$, in the plane normal to $\mathbf{v}$. The shear modulus can be expressed as

$$G(\mathbf{u}, \mathbf{v}) = (u_i v_j u_k v_l \mathsf{S}_{ijkl})^{-1}. \quad (8)$$

Similarly, Poisson's ratio $\nu(\mathbf{u}, \mathbf{v})$ which characterizes the transverse strain (in the $\mathbf{v}$ direction) under uniaxial stress (in the $\mathbf{u}$ direction), can be calculated as

$$\nu(\mathbf{u}, \mathbf{v}) = -\frac{u_i u_j v_k v_l \mathsf{S}_{ijkl}}{u_i u_j u_k u_l \mathsf{S}_{ijkl}}. \quad (9)$$

Both the shear modulus and Poisson's ratio, because they are functions of two orthogonal unit vectors and thus three scalar parameters, cannot be plotted directly in three dimensions.

III. RESULTS AND DISCUSSION

In our earlier work on this topic,[16] we compared the Young's and shear moduli of five flexible MOFs of the same framework topology to non-compliant MOFs ZIF-8 and MOF-5, whose elastic constants had already been reported in the literature. Here, we focus on three families of metal–organic frameworks, all built from parallel one-dimensional pillars interlinked by organic linkers and displaying the same overall "wine-rack" pattern, with one-dimensional lozenge-shaped pores. We analyze the mechanical properties of all three families, contrasting their behavior against one another. This allows us to delineate the elastic properties that are linked to framework compliance.

A. Compliant wine-rack: The MIL-53 family

The MIL-53 family is a subclass of MOF structures, first synthesized in Férey's group, that are made of parallel one-dimensional M(OH) chains (M = Al^{3+}, Ga^{3+}, Sc^{3+}, Fe^{3+}, Cr^{3+}, In^{3+}) linked together by 1,4-benzenedicarboxylate linkers to form linear diamond-shaped channels that are wide enough to accommodate small guest molecules. These materials may oscillate (or "breathe") between two different conformations called the large-pore phase (lp) and narrow-pore (np) phases which have a remarkable difference in cell volume of up to 40%. This family of materials also include functionalized variants of MIL-53, in which the organic linker has been modified (pre- or post-synthesis) to include additional functional groups. We also include in this family the material MIL-47, a MOF with similar structure to the MIL-53's large-pore phase, but whose pillar is a $V^{(IV)}O$ chain. It was recently demonstrated that MIL-47 undergoes a structural transition upon isotropic compression,[33] and it thus belongs to this "family." In this section, we discuss the mechanical properties of two materials from this family, MIL-53(Al) and MIL-47, which are summarized here in Table II. We have recently calculated the elastic constants of these structures, the first such calculation performed on soft porous crystals.[16] Here, we expand on the discussion of Ref. 16 by discussing the similarities and differences between the two materials' Young's modulus and shear modulus.

The three-dimensional representation of Young's modulus for MIL-53(Al)-lp and MIL-47 are presented in Fig. 3. We can see that they bear a striking resemblance, indicating that their near-identical framework topology is in a large part responsible for their mechanical properties, even though their coordination chemistry and the nature of their metal centers is different. First, both surfaces feature a large lobe along the axis of their inorganic chain (b axis for MIL-53(Al), a axis for MIL-47; their different space groups mean that their crystallographic axes do not coincide). This indicates a large stiffness along the inorganic chain. Second, they exhibit significant anisotropy, indicating that the material is "softer" with respect to compression in certain directions. Indeed, in the plane of the wine-rack motif (the plane perpendicular to the

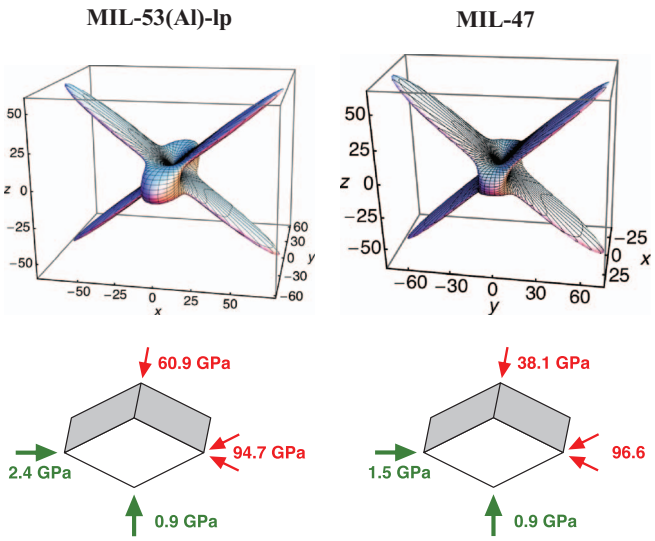

FIG. 3. (Top) directional Young's modulus for MIL-53(Al)-lp (left) and MIL-47 (right) represented as 3D surfaces, with axes tick labels in GPa. (Bottom) scheme of the Young modulus values for stiffest and softest directions, with Young's modulus values indicated.

inorganic chain: *ac* for MIL-53(Al), *bc* for MIL-47), there are both stiff directions (along the inorganic linkers) and "soft" directions (along the diagonals of the lozenge-shaped pore, which are aligned with the crystallographic axes). This very high anisotropy (two orders of magnitude!) is not present in non-flexible metal–organic frameworks such as MOF-5[9] and ZIF-8,[26] and is directly linked with the compliance of the MIL-53 wine-rack framework.

While the profiles of the directional Young's modulus of MIL-53(Al)-lp and MIL-47 are similar, they present some numerical differences (see Fig. 3) which are worth commenting on. In particular, their Young's modulus along the inorganic chain are different: $E_b = 60.9$ GPa for MIL-53(Al)-lp, while $E_a = 38.1$ GPa for MIL-47. This means that the Al(OH) chain is stiffer than the VO chain. On the other hand, the values of stiffness along the organic linkers are very close to one another (respectively, 94.7 and 96.6 GPa), indicating that the metal–organic coordination plays little role in these stiff compression directions. Finally, it is to be noted that the two "soft" directions of compression (*a* and *c* for MIL-53(Al), *b* and *c* for MIL-47) are not equivalent: there is a marked difference in Young's modulus between the two diagonal axes of the lozenge, with the greater diagonal associated with a larger modulus. This can be explained by the non-$\pi/2$ angle of the wine-rack motif: the greater diagonal is more aligned with the rigid organic ligands, making compression or expansion in this direction more difficult; oppositely, stress along the lesser diagonal is closer to being orthogonal to the ligands, and involves mostly weaker π-stacking interactions.

The anisotropy observed for the Young modulus of MIL-53(Al) and MIL-47 is, again, observed in their directional shear modulus and Poisson's ratio. We have already presented these results in Ref. 16, and we summarize them here again for clarity, because we will contrast them with the properties of MIL-122(In) and MIL-140A in Secs. III B and III C. Because both the shear modulus G and the Poisson ratio ν are functions of two orthogonal unit vectors $\mathbf{u}$ and $\mathbf{v}$, or equivalently a function of three scalar angles θ, ϕ, and χ, they cannot be plotted directly as a 3D surface. However, it can be seen from their maximal and minimal values (presented in Table II) that these properties show a strong anisotropy in both MIL-53(Al) and MIL-47. Again, the very similar values of shear modulus calculated for both materials indicate that their mechanical properties are linked mostly to the nature of their framework, rather than the details of their coordination chemistry. Furthermore, it is worth noting that anisotropy in a crystalline material's shear modulus is often linked to limited mechanical stability of said material. The existence of the unusually large anisotropy demonstrated here for the breathing MIL-53(Al) and MIL-47 frameworks allow us to hypothesize that they have very limited stability on the scale of the crystal in the presence of physical stimuli such as mechanical pressure, guest adsorption, or guest desorption. This is in keeping with the fact that, while relatively large monocrystals of MIL-53(Al) have been synthesized and reported in the literature, they transform into powders of sub-micrometer crystallites after activation or solvent evacuation.

As a conclusion, all compliant frameworks studied so far display:

- highly anisotropic Young's modulus and shear modulus, with some directions in the GPa or sub-GPa range;
- large anisotropy of their Poisson's ratio, including directions of negative Poisson's ratio;
- at least one direction of negative linear compressibility and one direction of large positive linear compressibility.

In Secs. III B and III C, we study other materials of wine-rack type frameworks, in order to see which of these features are associated with the wine-rack framework topology in general, and which are specific to the "breathing" of the frameworks.

B. Non-compliant wine-rack

We then turn our attention to the MIL-122(In) metal–organic framework.[34] Similarly, the MIL-53 structures, the framework of the MIL-122(M) materials (M = Al, Ga, or In) are based on M(OH) pillars, but in this case the pillars are linked together by 1,4,5,8-naphthalenetetracarboxylate ligands. The four-pronged nature of the linker and its X shape allow the overall framework to keep its wine-rack geometry (Figs. 1 and 4). However, because the naphthalenetetracarboxylate ligand is not itself flexible, half of the intersections in the wine-rack motif cannot act as hinges, while they all were in the compliant MIL-53 framework (Fig. 4). Thus, while the MIL-122 framework has a wine-rack geometry, we do not expect it to be compliant, i.e., undergo stimulus-induced large scale structural transitions. In fact, though the MIL-122 family has not yet been extensively studied, there has been no experimental indication of flexibility.

We report in Fig. 5, the 3D representation of the directional dependence of MIL-122(In)'s Young's modulus. There is a slight graphical similarity with that of MIL-53(Al)-lp and MIL-47 (Fig. 3) due wine-rack geometry of the framework. However, while MIL-122(In) displays clear anisotropy in its Young's modulus, it is two orders of magnitude lower (Table II). And most tellingly, the minimal value of the modulus is much higher, at 42.3 GPa, indicating that there is no soft deformation mode for uniaxial compression in this framework. This also holds true for the shear modulus, with again a lower anisotropy and higher absolute values that the compliant frameworks studied in Sec. III A. This confirms the link

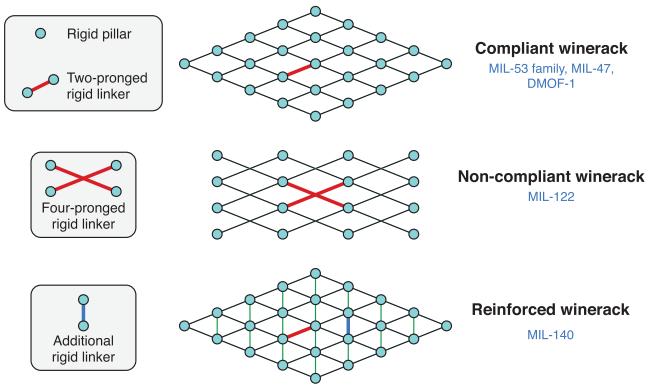

FIG. 4. Sketch of the three families of metal–organic frameworks exhibiting the wine-rack motif studied in this article.

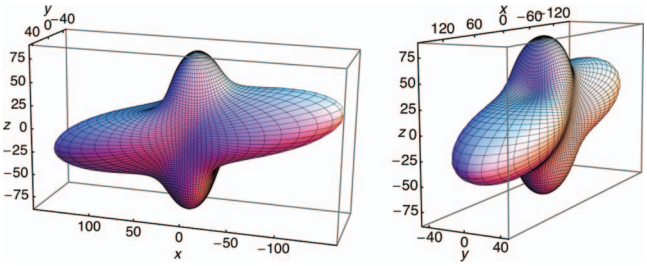

FIG. 5. Directional Young's modulus for MIL-122(In) represented as 3D surfaces, with axes tick labels in GPa.

between of soft (or "weak") deformation modes and large-scale structural transitions.

While it is clear from the analysis of MIL-122(In)'s Young's modulus and shear modulus that it is not a compliant framework, its wine-rack structure still has a clear impact on elastic properties: it presents both negative Poisson's ratio and negative linear compressibility. Both properties are linked to local deformations of the wine-rack structure, even after removal of half of its hinges. However, the scale of both the Poisson ration and linear compressibility variations is much smaller than for the compliant structures: β ranges from -1.9 TPa^{-1} to 17.5 TPa^{-1}, and ν ranges from -0.2 to 0.7 (Table II).

C. Reinforced wine-rack

Finally, a third type of framework we considered was that of the MIL-140 family.[35] These materials have complex zirconium oxide chains as inorganic subunits, interconnected to six other chains through the dicarboxylate linkers, which delimit pores of triangular cross-section: these can be seen as a "reinforced" wine-rack framework with higher coordination of the metal linkers (Fig. 4). Because of this change in connectivity between the inorganic chains, which act as the hinges of the wine-rack framework, the materials of the MIL-140 family would not be expected to present stimuli-induced structural transitions, though their flexibility has not been directly addressed in experimental studies so far.

The 3D representation of MIL-140A's directional Young's modulus is depicted in Fig. 6. It is surprisingly anisotropic, with a minimal value of $E_{\min} = 2.52$ GPa and a maximum of $E_{\max} = 81.1$ GPa (see Table II); its anisotropy $A_E \approx 31.8$ is therefore of the same order of magnitude to that of MIL-53(Al)-lp and MIL-47. However, upon closer inspection of the 3D surface representing MIL-140A's Young's modulus directional dependence, it appears that its overall shape and symmetry differ significantly from that of the simple wine-rack frameworks. Indeed, the variation of E in the Cartesian xy plane orthogonal to the inorganic ZrO zig-zag ladder (the "hinges" of the reinforced wine-rack framework, along the c axis) shows no "soft" direction: its minimum is $E_{\min}^{(xy)} \approx 31.3$ GPa. The direction of lowest stiffness is instead along lattice vector [0.05, -0.56, 0.83]. This vector, almost entirely in the yz plane, thus corresponds to a deformation mode involving the simultaneous expansion of the wine-rack motif along b, with no contraction along a but a contraction

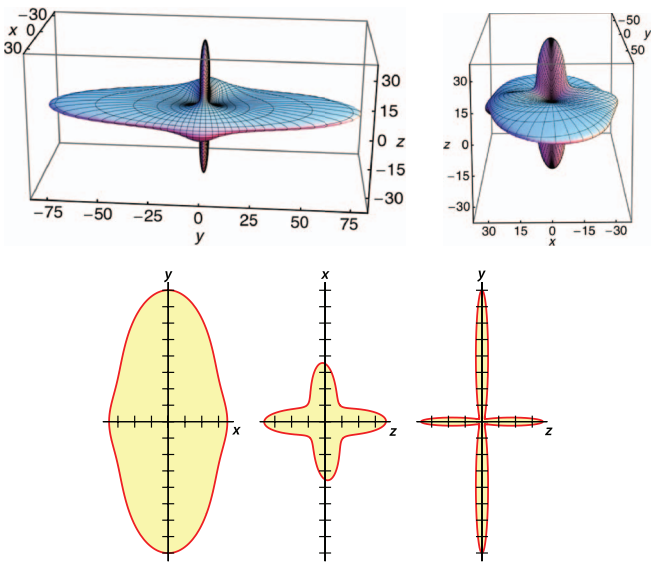

FIG. 6. Directional Young's modulus for MIL-140A represented as 3D surfaces (top), in the Cartesian xy, zx and zy planes (bottom; tick marks correspond to 10 GPa).

of the inorganic chain along the c. This uniaxial strain can be visualized in Fig. 7, and in the form of a movie as part of the supplementary material.[31] It is of a very different nature than that observed in the materials of the MIL-53 family, and is made possible by the compressibility of the double zig-zag ZrO ladder (Fig. 8). Unlike the simple Al(OH) and VO zig-zag ladders, the ZrO ladder itself bears a wine-rack motif and, as a consequence, is compliant. This, in turn, leads to an unexpected compliance of the overall MIL-140A framework that does rely solely on its "reinforced wine-rack" framework.

A similar conclusion can be reached from the analysis of the shear modulus, which also presents high anisotropy ($A_G \approx 36.2$) and a very low minimum of 0.65 GPa for a shearing involving the inorganic chain. However, we can see that the change in structure from MIL-53 to MIL-140, which is in effect a triangular framework, impacts the linear compressibility: in MIL-140A, β is positive in all directions, while it had negative lobes in other wine-rack-based frameworks. We

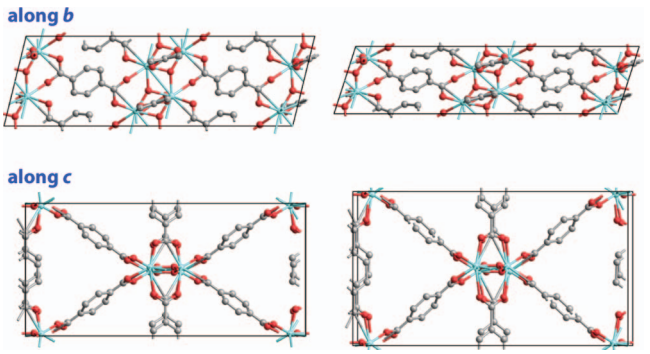

FIG. 7. Representation of uniaxial strain along the lattice vector [0.05, -0.56, 0.83] on the MIL-140A structure: the relaxed structure is on the left, a strain of +15% is depicted on the right. (Top) viewed along the b axis (a is horizontal, c is vertical); (bottom) viewed along the c axis (a is horizontal, b is vertical). This deformation is included in movie form in the supplementary material.[31]

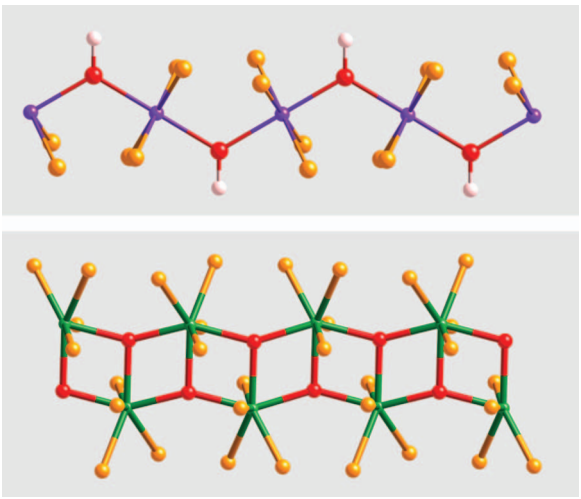

FIG. 8. Representation of the inorganic chains of MIL-53(Al)-lp (top; the chain is along the b axis) and MIL-140A (bottom; the chain is along the c axis). Zr: green; Al: purple; O: red; H: white; oxygen atoms of the linkers coordinating the metals are colored orange.

attribute this difference to the larger coordination number of the inorganic chains, which is 6 instead of 4 as in the MIL-53 and MIL-122 frameworks. In contrast, MIL-140A exhibits directions of negative Poisson's ratio. Those in fact correspond to the directions of soft Young's modulus, and to the deformation mode described in Fig. 7.

D. Existence of soft deformation modes: A simple criterion

In this paper, we have performed a full analysis of the elastic properties from the stiffness tensor C. We would like to note here that, if one's goal is merely to assess the existence of soft deformation modes, a simpler approach is possible. The elastic energy for a given strain, $E(\varepsilon)$, can be expressed as

$$E(\varepsilon) = \frac{1}{2}\varepsilon : \mathsf{C} : \varepsilon = \frac{1}{2}\sum_{ijkl} \mathsf{C}_{ijkl}\varepsilon_{ij}\varepsilon_{kl}. \qquad (10)$$

The Born stability condition for the relaxed crystal requires that this energy be positive, i.e., $\varepsilon \neq 0 \Rightarrow E(\varepsilon) > 0$. This quadratic form is definite positive if, and only if, the eigenvalues of C are all positive.[32] Similarly, we can define the softest deformation mode as the unit strain ε_0 yielding the smallest energy,

$$\min_{\|\varepsilon\|=1} \left(\sum_{ijkl} \mathsf{C}_{ijkl}\varepsilon_{ij}\varepsilon_{kl} \right). \qquad (11)$$

This, in turn, corresponds to the eigenvector of C corresponding to the smallest eigenvalue. Thus, the existence of a small eigenvalue indicates the existence of a soft deformation mode. The associated eigenvector indicates the nature of the mode (normal and shear components). As can be checked on Table III, this correlates well with the more exhaustive study of Young's and shear moduli.

TABLE III. Eigenvalues λ_i (in GPa) of the stiffness matrix C of the MOFs studied in this work.

Structure	λ_1	λ_2	λ_3	λ_4	λ_5	λ_6
MIL-53(Al)-lp	0.66	7.24	8.27	39.5	57.0	132.1
MIL-47	0.57	7.76	9.30	36.7	50.8	102.1
MIL-122(In)	15.2	19.3	26.1	42.8	84.0	228.7
MIL-140A	0.65	3.92	16.3	24.7	55.4	108.1

IV. CONCLUSION

We performed first principles calculations of the elastic constants of metal–organic frameworks based on the wine-rack framework topology, and detailed how to derive mechanical properties such as Young's modulus, shear modulus, Poisson's ratio, and linear compressibility. We showed that framework compliance, as attested by the existence of deformation modes of very low rigidity, is linked to directions of low Young's modulus or shear modulus. In turn, we proposed to use the smallest eigenvalue of the positive definite stiffness matrix as a measure of this compliance. We showed how the full tensorial analysis of the mechanical behavior of wine-rack-based MOFs in the elastic regime offers insight into their compliance and opens up new opportunities for better understanding and tuning their mechanical properties. In particular, we predict on this basis that the MIL-140A material can exhibit unexpected framework compliance in a deformation mode involving compression of the inorganic ZrO double zig-zag ladder, a feature that has not yet been evidenced experimentally.

ACKNOWLEDGMENTS

The authors thank Bartolomeo Civalleri for early access to the 2.0.1 update of the CRYSTAL09 code, as well as insightful comments about the quantum chemistry calculations of elastic constants. This work was supported by the Agence Nationale de la Recherche under project "SOFT-CRYSTAB" (ANR-2010-BLAN-0822), and performed using HPC resources from GENCI-IDRIS (Project Nos. 086114 and 087069).

[1] S. Horike, S. Shimomura, and S. Kitagawa, Nat. Chem. **1**, 695 (2009).
[2] G. Férey and C. Serre, Chem. Soc. Rev. **38**, 1380 (2009).
[3] F. Millange, C. Serre, N. Guillou, G. Férey, and R. I. Walton, Angew. Chem., Int. Ed. **47**, 4100 (2008).
[4] C. Mellot-Draznieks, J. Mater. Chem. **17**, 4348 (2007).
[5] F. Salles, G. Maurin, C. Serre, P. L. Llewellyn, C. Knöfel, H. J. Choi, Y. Filinchuk, L. Oliviero, A. Vimont, J. R. Long, and G. Férey, J. Am. Chem. Soc. **132**, 13782 (2010).
[6] A. M. Walker, B. Civalleri, B. Slater, C. Mellot-Draznieks, F. Corà, C. M. Zicovich-Wilson, G. Román-Pérez, J. M. Soler, and J. D. Gale, Angew. Chem., Int. Ed. **49**, 7501 (2010).
[7] S. Watanabe, H. Sugiyama, H. Adachi, H. Tanaka, and M. Miyahara, J. Chem. Phys. **130**, 164707 (2009).
[8] F.-X. Coudert, A. Boutin, M. Jeffroy, C. Mellot-Draznieks, and A. H. Fuchs, ChemPhysChem **12**, 247 (2011).
[9] D. Bahr, J. Reid, W. Mook, C. Bauer, R. Stumpf, A. Skulan, N. Moody, B. Simmons, M. Shindel, and M. Allendorf, Phys. Rev. B **76**, 184106 (2007).
[10] M. Tafipolsky, S. Amirjalayer, and R. Schmid, J. Phys. Chem. C **114**, 14402 (2010).

[11]A. V. Neimark, F.-X. Coudert, A. Boutin, and A. H. Fuchs, J. Phys. Chem. Lett. **1**, 445 (2010).
[12]I. Beurroies, M. Boulhout, P. L. Llewellyn, B. Kuchta, G. Férey, C. Serre, and R. Denoyel, Angew. Chem., Int. Ed. **49**, 7526 (2010).
[13]A. V. Neimark, F.-X. Coudert, C. Triguero, A. Boutin, A. H. Fuchs, I. Beurroies, and R. Denoyel, Langmuir **27**, 4734 (2011).
[14]Q. Ma, Q. Yang, A. Ghoufi, G. Férey, C. Zhong, and G. Maurin, Dalton Trans. **41**, 3915 (2012).
[15]P. Serra-Crespo, E. Stavitski, F. Kapteijn, and J. Gascon, RSC Adv. **2**, 5051 (2012).
[16]A. U. Ortiz, A. Boutin, A. H. Fuchs, and F.-X. Coudert, Phys. Rev. Lett. **109**, 195502 (2012).
[17]J. M. Ogborn, I. E. Collings, S. A. Moggach, A. L. Thompson, and A. L. Goodwin, Chem. Sci. **3**, 3011 (2012).
[18]R. H. Baughman, S. Stafström, C. Cui, and S. O. Dantas, Science **279**, 1522 (1998).
[19]A. B. Cairns, A. L. Thompson, M. G. Tucker, J. Haines, and A. L. Goodwin, J. Am. Chem. Soc. **134**, 4454 (2012).
[20]W. Li, M. R. Probert, M. Kosa, T. D. Bennett, A. Thirumurugan, R. P. Burwood, M. Parinello, J. A. K. Howard, and A. K. Cheetham, J. Am. Chem. Soc. **134**, 11940 (2012).
[21]R. Dovesi, R. Orlando, B. Civalleri, C. Roetti, V. R. Saunders, and C. M. Zicovich-Wilson, Z. Kristallogr. **220**, 571 (2005).
[22]A. D. Becke, J. Chem. Phys. **98**, 5648 (1993).
[23]S. Grimme, J. Comput. Chem. **27**, 1787 (2006).
[24]D. W. Lewis, A. R. Ruiz-Salvador, A. Gómez, L. M. Rodriguez-Albelo, F.-X. Coudert, B. Slater, A. K. Cheetham, and C. Mellot-Draznieks, CrystEngComm **11**, 2272 (2009).
[25]W. Perger, J. Criswell, B. Civalleri, and R. Dovesi, Comput. Phys. Commun. **180**, 1753 (2009).
[26]J.-C. Tan, B. Civalleri, C.-C. Lin, L. Valenzano, R. Galvelis, P.-F. Chen, T. Bennett, C. Mellot-Draznieks, C. Zicovich-Wilson, and A. Cheetham, Phys. Rev. Lett. **108**, 095502 (2012).
[27]J. F. Nye, *Physical Properties of Crystals—Their Representation by Tensors and Matrices* (Clarendon, 1985).
[28]Depending on the system's space group, some deformations may be equivalent and thus fewer than 6 deformation modes will have to be considered. In the case of the orthorhombic and monoclinic lattices studied here, all six deformations are needed.
[29]A. Marmier, Z. A. D. Lethbridge, R. I. Walton, C. W. Smith, S. C. Parker, and K. E. Evans, Comput. Phys. Commun. **181**, 2102 (2010).
[30]Wolfram Research, Inc., *Mathematica*, Version 9.0, Champaign, IL, 2012.
[31]See supplementary material at http://dx.doi.org/10.1063/1.4802770 for the tensorial analysis code of the second-order elastic constants and visualization of the strain of lowest Young's modulus in MIL-140A.
[32]J. W. Morris, Jr. and C. R. Krenn, Philos. Mag. A **80**, 2827 (2000).
[33]P. G. Yot, Q. Ma, J. Haines, Q. Yang, A. Ghoufi, T. Devic, C. Serre, V. Dmitriev, G. Férey, C. Zhong, and G. Maurin, Chem. Sci. **3**, 1100 (2012).
[34]C. Volkringer, T. Loiseau, N. Guillou, G. Férey, and E. Elkaïm, Solid State Sci. **11**, 1507 (2009).
[35]V. Guillerm, F. Ragon, M. Dan-Hardi, T. Devic, M. Vishnuvarthan, B. Campo, A. Vimont, G. Clet, Q. Yang, G. Maurin, G. Férey, A. Vittadini, S. Gross, and C. Serre, Angew. Chem., Int. Ed. **51**, 9267 (2012).